Characterization of KCNQ1 atrial fibrillation mutations reveals distinct dependence on KCNE1

Priscilla J. Chan,[1] Jeremiah D. Osteen,[1] Dazhi Xiong,[1] Michael S. Bohnen,[1] Darshan Doshi,[2] Kevin J. Sampson,[1] Steven O. Marx,[1,2] Arthur Karlin,[3,4] and Robert S. Kass[1]

[1]Department of Pharmacology and [2]Department of Medicine, College of Physicians and Surgeons; [3]Department of Biochemistry and Molecular Biophysics, and [4]Department of Physiology and Cellular Biophysics, Columbia University Medical Center, New York, NY 10032

The I_{Ks} potassium channel, critical to control of heart electrical activity, requires assembly of α (KCNQ1) and β (KCNE1) subunits. Inherited mutations in either I_{Ks} channel subunit are associated with cardiac arrhythmia syndromes. Two mutations (S140G and V141M) that cause familial atrial fibrillation (AF) are located on adjacent residues in the first membrane-spanning domain of KCNQ1, S1. These mutations impair the deactivation process, causing channels to appear constitutively open. Previous studies suggest that both mutant phenotypes require the presence of KCNE1. Here we found that despite the proximity of these two mutations in the primary protein structure, they display different functional dependence in the presence of KCNE1. In the absence of KCNE1, the S140G mutation, but not V141M, confers a pronounced slowing of channel deactivation and a hyperpolarizing shift in voltage-dependent activation. When coexpressed with KCNE1, both mutants deactivate significantly slower than wild-type KCNQ1/KCNE1 channels. The differential dependence on KCNE1 can be correlated with the physical proximity between these positions and KCNE1 as shown by disulfide cross-linking studies: V141C forms disulfide bonds with cysteine-substituted KCNE1 residues, whereas S140C does not. These results further our understanding of the structural relationship between KCNE1 and KCNQ1 subunits in the I_{Ks} channel, and provide mechanisms for understanding the effects on channel deactivation underlying these two atrial fibrillation mutations.

INTRODUCTION

I_{Ks} is the slowly activating component of delayed rectifier K^+ current in the heart and is a major contributor to the timing of repolarization of the cardiomyocyte membrane potential (Sanguinetti and Jurkiewicz, 1990). The I_{Ks} channel is composed of a tetramer of pore-forming α subunits, KCNQ1 (Q1), and accessory β subunits, KCNE1 (E1; Barhanin et al., 1996; Sanguinetti et al., 1996). Mutations in either KCNQ1 or KCNE1 have been linked to cardiac arrhythmia syndromes, including long QT syndrome (LQTS; Splawski et al., 2000), short QT syndrome (SQTS; Bellocq et al., 2004), and familial atrial fibrillation (FAF; Chen et al., 2003; Hong et al., 2005; Lundby et al., 2007; Das et al., 2009).

The biophysical properties of I_{Ks} channel current are dramatically altered when KCNE1 associates with the KCNQ1 channel. Functional tetrameric channels can be formed by KCNQ1 alone, but coassembly with KCNE1 is required for the unique kinetics necessary to regulate human cardiac electrical activity as well as for the channel's functional response to the sympathetic nervous system. Specifically, KCNE1 coassembly results in a depolarizing shift in the voltage dependence

of activation, an increase in the single channel conductance, and an increase in current density (Barhanin et al., 1996; Sanguinetti et al., 1996; Sesti and Goldstein, 1998). I_{Ks} channel current is also characterized by slow activation and deactivation kinetics, with little or no inactivation, in contrast to the KCNQ1 homomeric channel, which is characterized by fast activation and deactivation kinetics and clear inactivation (Tristani-Firouzi and Sanguinetti, 1998).

Recent studies reporting spontaneous cross-linking between substituted cysteine residues on KCNE1 and KCNQ1 have positioned KCNE1 between the first and sixth transmembrane helices (S1 and S6, respectively) of opposing KCNQ1 subunits, which is consistent with the current KCNQ1 structural model (Kang et al., 2008; Xu et al., 2008; Chung et al., 2009). In this region of S1, two gain-of-function disease mutations associated with atrial fibrillation (AF), S140G and V141M, are located in adjacent residues. When KCNQ1 containing either AF-related mutation in S1 (S140G or V141M) is coexpressed heterologously with KCNE1, the resultant channels activate immediately in response to depolarizing pulses applied from holding potentials similar to typical

myocyte resting potentials (Chen et al., 2003; Hong et al., 2005). Subsequent analysis has revealed that the instantaneous current is caused by accumulation of open channels, which is caused by incomplete deactivation between pulses at these holding potentials (Restier et al., 2008). To date, this channel property is believed to be manifested only in the presence of KCNE1 for both mutations (Restier et al., 2008).

Here we have explored the roles of KCNE1 in translating the effects of the KCNQ1 AF mutations S140G and V141M into pathological channel function by characterizing the mutations in the absence and presence of KCNE1. We have explored the structural proximity of KCNE1 relative to the two AF mutations located in S1 KCNQ1 by using a biochemical assay to look for disulfide bridge formation between introduced cysteines. Our results demonstrate that even though both mutations exhibit extremely slow deactivation kinetics in the presence of KCNE1, they have distinct dependencies on this accessory subunit. V141M KCNQ1 channels resemble wild-type (WT) KCNQ1 channels in the absence of KCNE1; thus, coassembly with KCNE1 is required to alter channel deactivation kinetics. However, the S140G mutation in KCNQ1 itself is sufficient to dramatically slow the deactivation process, and coassembly with KCNE1 further slows channel closing. Biochemical evidence correlates function with structure, revealing orientation of the two proteins such that KCNQ1 V141, but not S140, is positioned close to KCNE1, providing a structural basis for distinct subunit dependence of channel function conferred by these two AF mutations. In line with the prediction of a direct interaction between V141M and KCNE1, we demonstrate that the location of KCNE1 within a heterozygous channel complex impacts the severity of the mutant phenotype. Our results support the notion of a physiologically important interaction between KCNE1 and KCNQ1 S1, sensitive to mutation, that dramatically affects the rate of channel deactivation.

MATERIALS AND METHODS

Molecular biology and cell culture

Human KCNE1 (Murai et al., 1989) was subcloned into the p3XFLAG-CMV-14 expression vector (E4901; Sigma-Aldrich) to generate a C-terminal FLAG-tagged KCNE1. Mutations were engineered into human KCNQ1 (Sanguinetti et al., 1996) and KCNE1 cDNA with the QuikChange site-directed mutagenesis kit (Agilent Technologies). All biochemical experiments were conducted with these constructs. Human KCNE1 with an N-terminal HA tag was used for functional studies. A tandem construct, EQQ, was generated using a previously tested fusion construct, E1-Q1 (Wang et al., 1998). E1-Q1 construct was engineered by linking the C terminus of KCNE1 to the N terminus of KCNQ1. Next, the EQQ construct was engineered by inserting an additional KCNQ1 subunit into the E1-Q1 construct. The E1-Q1 and Q1 dimer constructs were digested with XhoI, and the 2-kb insert from the Q1 dimer was gel-purified and ligated into the XhoI site of E1-Q1. The nomenclature used is to reflect the individual subunits engineered into the construct; EQQ indicates one KCNE1

subunit linked to two KCNQ1 subunits. The human rhinovirus (HRV-3C) protease (EMD) consensus cleavage site, LEVLFQGP, which is cleaved between the Q and G, was inserted into the C terminus of KCNE1 to create a cleavage site between KCNE1 and KCNQ1 (Liu et al., 2008a).

Chinese hamster ovary (CHO) cells (American Type Culture Collection) were cultured in Ham's F-12 culture media with 10% FBS in a 37°C incubator with 5% CO_2.

Electrophysiology

CHO cells were transfected with WT or mutant KCNQ1 alone or cotransfected with WT or mutant KCNE1, as well as with eGFP (0.4 µg of each cDNA), and then plated on 35 × 10-mm tissue culture dishes as described previously (Marx et al., 2002). Electrophysiological measurements were performed 48 h after transfection. Currents were recorded at 25°C using the whole-cell patch clamp configuration with an Axopatch 200A amplifier (Molecular Devices) as described previously (Kurokawa et al., 2003). Series resistance was 2–3 MΩ. The physiological K^+ external solution contained 132 mM NaCl, 4.8 mM KCl, 1.2 mM $MgCl_2$, 1 mM $CaCl_2$, 5 mM glucose, and 10 mM Hepes; pH was adjusted to 7.4 with NaOH. Internal solution contained 110 mM K^+ aspartate, 1 mM $MgCl_2$, 1 mM $CaCl_2$, 11 mM EGTA, 5 mM K_2ATP, and 10 mM HEPES. Cells were chosen based on eGFP fluorescence. For experiments in elevated K^+, external solution contained 17.8 mM NaCl, 120 mM KCl, 1.2 mM $MgCl_2$, 1 mM $CaCl_2$, 5 mM glucose, and 10 mM HEPES; pH was adjusted to 7.4 with NaOH.

Voltage clamp protocols

To record the conductance–voltage (G-V) relationship for I_{Ks}, cells were voltage clamped at a negative holding potential (−80, −100 mV, or −120 mV). Test potentials were applied to a series of isochronal (2 s) activation voltages with a fixed incremental increase between successive pulses (e.g., −100 to +40 mV in 20-mV steps). Activation was determined from the amplitude of deactivating tail currents measured at voltages indicated in the text for specific experiments as a function of the preceding test pulse voltage. The interval between test pulses was 15 or 20 s, as described in the figure legends.

To compare activation kinetics of channels with differing voltage dependences, voltages were chosen where open probabilities were similar. Time to half activation ($t_{1/2}$) was measured during 2-s pulses, taken at the voltage closest to the $V_{1/2}$ acquired from the G-V relationship for each subunit combination. Time to half activation, $t_{1/2}$, is measured with the relation to the maximal current in the corresponding 2-s test pulse.

Unless otherwise indicated, kinetics of deactivating tail currents were analyzed using 2-s depolarizing steps to +20 mV applied every 15 s from a −100 mV holding potential followed by 2-s repolarizing steps ranging from −80 to −120 mV (20-mV increments). The time constant of I_{Ks} deactivation (τ_{deact}) measured at −80mV, −100 mV, and −120 mV was obtained by fitting tail currents with unconstrained single exponential functions.

Cross-linking

Cross-linking procedures and the calculation of the cross-linking percentage have been described previously (Chung et al., 2009). CHO cells were cotransfected with mutant cDNAs of KCNQ1 C136V-C214A-C331A (pWTKCNQ1) and FLAG-KCNE1 (1.0 µg each) using PLUS reagent and Lipofectamine (Invitrogen). Cells were incubated for 48 h at 37°C in the presence of 5% CO_2.

Cross-linking occurred in the presence of ambient oxygen, and no external oxidizing agents were added, as described previously (Chung et al., 2009). To study only surface membrane proteins, the adherent cells were surface-biotinylated with EZ-Link Sulfo-NHS-LC-Biotin (Thermo Fisher Scientific), the reaction was stopped with glycine methyl ester, the cells were lysed, and, after

sedimentation of insoluble material, the supernatant was mixed with Ultralink Immobilized NeutrAvidin Protein Plus beads (Thermo Fisher Scientific) to bind the biotin-labeled membrane proteins. These were eluted from the beads by exposure for 3 min at 90°C to 8 M urea, 4% SDS, 200 mM Tris, pH 8.0, and 2 mM EDTA, all as described previously (Liu et al., 2008b). Dithiothreitol (DTT) to a final concentration of 20 mM was added to half of each eluate. Samples were incubated at 50°C for 20 min, bromophenol blue was added, and the samples in SDS sample buffer were electrophoresed on 4–20% acrylamide gels. The gels were transferred to nitrocellulose, and the blot was blocked with blocking buffer for near infrared fluorescent Western blotting (Rockland Immunochemicals Inc.) and incubated with goat anti–KCNQ1 C-20 antibody (1:1,000; Santa Cruz Biotechnology, Inc.) and mouse anti-FLAG M2 antibody (1:2,000; Sigma-Aldrich). Membranes were washed and incubated with donkey anti–goat Alexa Fluor 680–labeled antibody (1:5,000; Invitrogen) and donkey anti–mouse IRDye 800–labeled antibody (1:5,000; LI-COR Biosciences). Fluorescent signals were detected using the Odyssey Infrared Imager (LI-COR).

The extent of cross-linking was calculated as follows: (KCNQ1/KCNE1 + X/2)/(KCNQ1/KCNE1 + KCNQ1 + KCNQ1$_2$ + X). Calculations were based on the intensities of four bands: the monomeric KCNQ1 band ($\sim$74 kD), the cross-linked KCNQ1/KCNE1 band ($\sim$110 kD), the KCNQ1$_2$ band (KCNQ1 dimer $\sim$150 kD), and a band labeled X ($\sim$250 kD; Fig. S3; Chung et al., 2009).

2-aminoethyl methanethiosulfonate hydrobromide (MTSEA)-biotin experiments

To verify that the S140C was accessible for cross-linking to Cys-KCNE1 residues, MTSEA-biotin (Biotium) was used to assay the reactivity of this residue. MTSEA-biotin was dissolved in DMSO at a concentration of 2 mg/100 µl and then diluted with PBS at a ratio of 1 to 100. A final concentration of 0.5 mM MTSEA-biotin solution was added to the external bath solution. In these experiments, peak currents were measured at the end of a 2-s depolarizing pulse to +60 mV and normalized to capacitance.

Data analysis

Data were collected using Clampex 8.0 (Molecular Devices) and analyzed as described previously (Kurokawa et al., 2003) with Clampfit 8.0 (Molecular Devices) and Origin 7.0 (OriginLab Corp). Statistical data analysis was assessed with a Student's t test; differences at P < 0.05 were considered to be significant.

Online supplemental material

Fig. S1 verifies that WT I$_{Ks}$ currents exhibited similar activation and deactivation properties in both physiological K$^+$ (5 mM) and elevated K$^+$ (120 mM) external solutions. Fig. S2 confirms that the S140C residue is available to cross-link by applying a charged MTS reagent. Fig. S3 contains a full-length Western blot of cross-linking bands illustrating the methodology of cross-link quantification. Fig. S4 demonstrates the functional consequences of cross-linking for cysteine pair V141C–A44C in the absence and presence of DTT. Fig. S5 demonstrates the functional consequences of individual cysteine mutations on channel function in the absence and presence of DTT. Fig. S6 shows that the HRV-3C site introduced to the EQ dimer is efficiently cleaved by proteolysis. Online supplemental material is available at http://www.jgp.org/cgi/content/full/jgp.201110672/DC1.

RESULTS

### S140G, but not V141M, slows deactivation of homomeric channels

To probe the impact of KCNE1 on S140G and V141M mutant phenotypes, we first characterized the functional

effects of these mutations in cells expressing channels encoded by the KCNQ1 subunit alone (Fig. 1, A–C). Because we were interested in determining the influence of each of these mutations on channel deactivation, particularly over a negative range of voltages, experiments were performed in external solutions containing elevated K$^+$ concentration (120 mM, see Materials and methods). Control experiments (Fig. S1) verified that elevated K$^+$ did not affect the voltage-dependence and deactivation of the KCNQ1 channel compared with experiments in physiological K$^+$ solution (5 mM). As had been shown for V141M channels in *Xenopus laevis* oocytes (Hong et al., 2005), we find that channels encoded by both S140G and V141M close if voltages are sufficiently negative. Once closed, channels were then opened by application of positive test pulses. There was no significant difference in the V$_{1/2}$ of activation obtained for WT KCNQ1 (V$_{1/2}$ = $-29 \pm$ 2.1 mV, n = 4) and V141M channels (V$_{1/2}$ = -29 ± 0.9 mV, n = 5, P > 0.05 vs. WT KCNQ1); however, the V$_{1/2}$ of activation for S140G channels is significantly more negative than WT KCNQ1 channels (V$_{1/2}$ = -57 ± 1.3 mV; n = 5; P < 0.05 vs. WT KCNQ1; Fig. 1 D). S140G channels also exhibited significantly slower deactivation over a range of voltages from -80 to -120 mV compared with WT KCNQ1 and V141M channels (Fig. 1 E and Table 1).

KCNE1 co-assembly with S140G and V141M mutations reveals a preferential effect on deactivation kinetics versus activation kinetics

We next investigated the impact of KCNE1 on channel properties when coexpressed with KCNQ1 carrying either of these two disease-associated mutations. A pulse protocol consisting of 2-s isochronal activating pulses to +20 mV was applied at a very slow rate (once every 20 s) to ensure that the majority of channels were closed between pulses. We next measured the impact of KCNE1 coexpression on activation gating. Representative current traces for S140G and V141M, assembled with KCNE1, reveal channels that exhibit the slow onset of activation seen in WT I$_{Ks}$ channels (Fig. 2, A–C). The voltages for half maximal (isochronal) activation for channels consisting of KCNE1 coexpressed with three KCNQ1 variants were measured to compare voltage dependence of activation gating (KCNQ1/KCNE1: V$_{1/2}$ = 17.5 $\pm$ 2.6 mV, n = 6; S140G/KCNE1: V$_{1/2}$ = 1.5 $\pm$ 2.7 mV, n = 4; V141M/KCNE1: V$_{1/2}$ = 2.4 $\pm$ 1.0 mV, n = 3; Fig. 2 D). I$_{Ks}$ activation kinetics were then compared by measuring the time ($t_{1/2}$) at which I$_{Ks}$ current is half maximally activated at the voltage closest to the V$_{1/2}$ for each subunit combination. KCNE1 coexpression caused no significant change in activation kinetics of the S140G ($t_{1/2}$ = 1.5 $\pm$ 0.04 s, n = 4) and V141M ($t_{1/2}$ = 1.45 $\pm$ 0.06 s, n = 4) assembled channels (P > 0.05 for S140G/KCNE1 vs. V141M/KCNE1). Although both were significantly different from WT KCNQ1/KCNE1 channels

Figure 1. S140G, but not V141M, slows deactivation of homomeric channels. (A–C) Representative families of current traces in cells expressing KCNQ1 (A), S140G (B), and V141M (C) in the absence of KCNE1. Currents are in response to 2-s pulses from −100 mV to +40 mV in 20-mV increments from a −100-mV holding potential. (D) Normalized isochronal (2 s) activation curves for KCNQ1 (squares), S140G (circles), and V141M (triangles). (E) Deactivation time constant (tau) obtained at voltages from −80 to −120 mV from single exponential fits to tail currents after a common depolarization (+20 mV, 2 s). For all current traces, the vertical scale is 50 pA/pF and the horizontal scale is 1.0 s. Data are shown as mean ± SEM (error bars). *, P < 0.05.
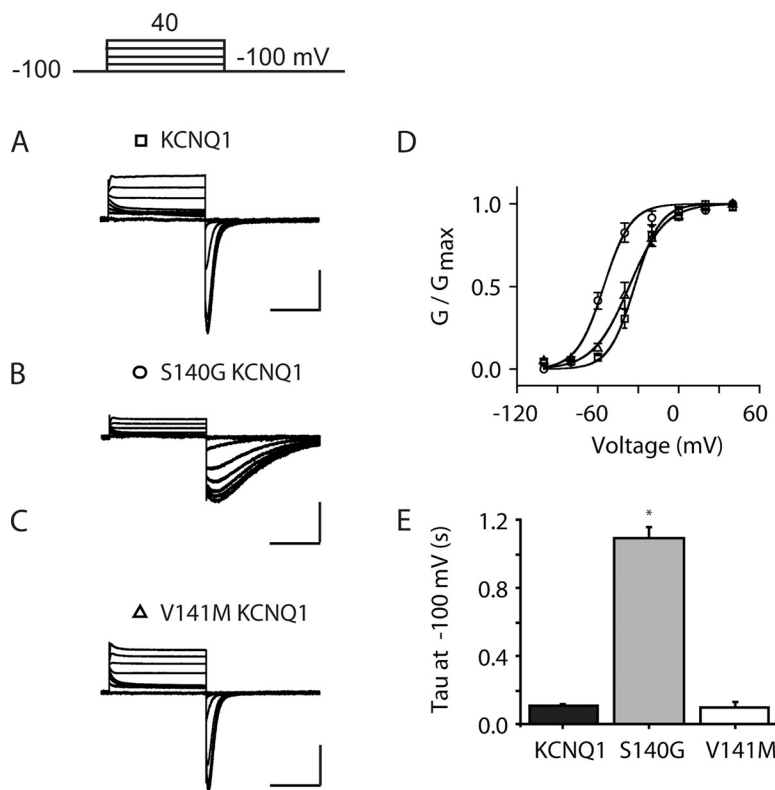
($t_{1/2}$ = 1.15 ± 0.31 s, n = 6), this was a small difference that did not take away from our main focus, which was to look for changes in deactivation kinetics (Fig. 2 E).

We next focused on deactivation kinetics of the S140G and V141M mutant channels in the presence of KCNE1. To compare deactivation for the different KCNQ1/KCNE1 pairs, we determined the deactivation time constants by measuring tail currents at −120 mV after 2-s depolarizing pulses (Fig. 3, A and B). The deactivation time constant for S140G/KCNE1 channels (τ_{deact} = 4.09 ± 0.23 s, n = 5) is significantly greater than that for WT KCNQ1/KCNE1 channels (τ_{deact} = 0.24 ± 0.004 s, n = 6, P < 0.05 for S140G/KCNE1 vs. WT KCNQ1/KCNE1). For V141M/KCNE1 channels, deactivation is significantly slower than both WT KCNQ1 and S140G channels assembled with KCNE1 (τ_{deact} = 6.71 ± 0.64 s, n = 4, P < 0.05 vs. WT KCNQ1/KCNE1 and P < 0.05 vs. S140G/KCNE1; Fig. 3 C).

Another way to analyze the KCNE1 functional interaction with S140G and V141M in terms of slowing deactivation is by examining the ratio of deactivation tau between the KCNQ1 subunit alone and coexpression with KCNE1. For the WT KCNQ1 channel, deactivation at −120mV is slowed about threefold in the presence of KCNE1 (Fig. 3 C). For KCNQ1 S140G, a slightly larger change in deactivation tau is seen from the addition of KCNE1 of about sevenfold. In contrast, KCNE1 coexpression with V141M subunits reveals a much more dramatic effect, slowing deactivation by >50-fold (KCNQ1, 2.74 ± 0.14; S140G, 7.75 ± 0.99; V141M, 51.39 ± 5.57; Fig. 3 C).
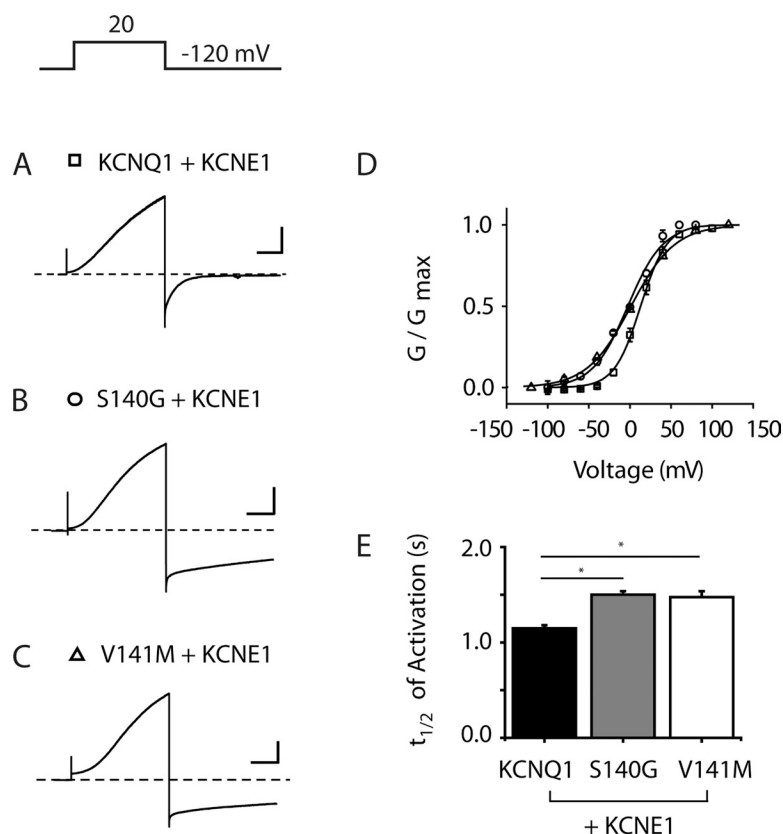
Cross-linking of substituted cysteines in KCNQ1 and KCNE1 provides a structural basis for functional data

The functional data suggest possible physical differences in the location of KCNQ1 residues S140 and V141 relative to KCNE1 in assembled channels. We thus sought to determine the proximity of S140 and V141 to KCNE1 by individually substituting cysteines in KCNQ1 and KCNE1 and monitoring spontaneous disulfide bridge

TABLE 1

τ of deactivation at different voltages for KCNQ1 S1 mutants

Construct	Tau at −80 mV	Tau at −100 mV	Tau at −120 mV
WT KCNQ1	131 ± 31	104 ± 3	82 ± 14
KCNQ1 S140G	2,240 ± 160[a]	1,090 ± 71[a]	666 ± 110[a]
KCNQ1 V141M	153 ± 18	101 ± 32	80 ± 28

Data presented as mean tau of deactivation from exponential fit ± SEM (n = 4–6).
[a]The tau of deactivation is significantly different from WT at the indicated voltage.

Figure 2. S140G and V141M minimally affect KCNQ1/KCNE1 activation kinetics. (A–C) Representative current traces are shown for KCNQ1, S140G, and V141M, each coexpressed with KCNE1. Holding potential $= -80$ mV (KCNQ1) and -100 mV (S140G and V141M). Cells were pulsed to -120 mV (KCNQ1 and S140G) and -140 mV (V141M) to ensure that all channels were closed before the depolarizing pulse ($+20$ mV, 2 s). (D) Normalized isochronal (2 s) activation curves for KCNQ1 (squares), S140G (circles), and V141M (triangles). (E) Activation $t_{1/2}$ for KCNQ1, S140G, and V141M. For all current traces, the vertical scale is 100 pA/pF and the horizontal scale is 0.5 s. Broken lines indicate zero current. Data are shown as mean ± SEM (error bars). *, $P < 0.05$.

formation (Fig. 4 A). To compare our results with the functional data, we specifically assayed cross-linking of membrane proteins, as described in Materials and methods. Two KCNQ1 Cys-substituted mutants (S140C and V141C) and 12 KCNE1 Cys-substituted mutants

(G40C to L51C) were generated. These KCNE1 residues were chosen for cysteine substitution because of their location in the region of KCNE1, which is predicted to be aligned with the region where Ser 140 and Val 141 are located (Kang et al., 2008; Chung et al., 2009).
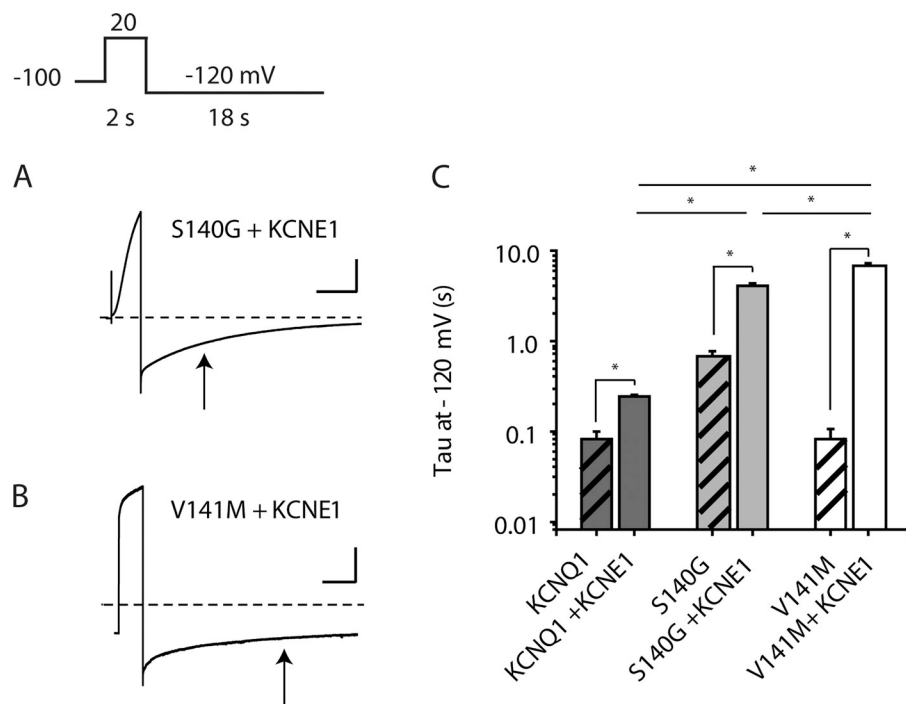

Figure 3. KCNE1 slows deactivation of V141M heteromeric channels to a greater extent than S140G channels. (A) Representative current traces are shown for S140G and V141M, each coexpressed with KCNE1. Arrows indicate the tau for each subunit combination. (B) Deactivation time constant (tau) at -120 mV is represented in a log plot for KCNQ1, S140G, and V141M, each coexpressed with and without KCNE1 ($n = 4$–5). (C) Hatched bars represent KCNQ1, S140G, and V141M without KCNE1. For S140G/KCNE1 and V141M/KCNE1 current traces, the vertical scale is 50 pA/pF and 100 pA/pF, respectively; the horizontal scale is 2.5 s. Broken lines indicate zero current. Data are shown as mean ± SEM (error bars). *, $P < 0.05$.
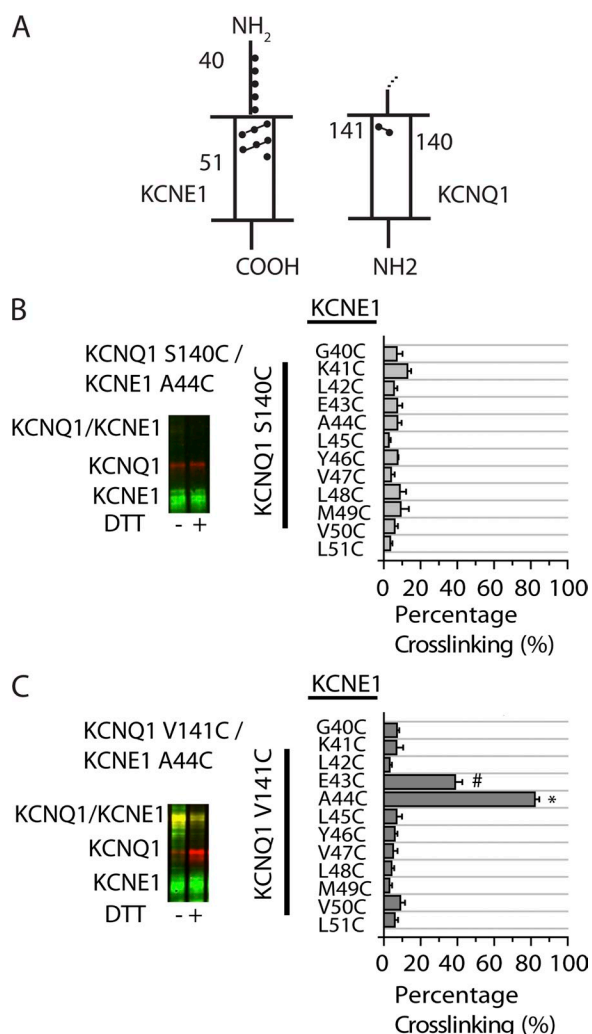
Chan et al.   139

Figure 4. Cross-linking of substituted cysteines in KCNQ1 and KCNE1 reveals the orientation of S140 and V141 relative to KCNE1. (A) Schematic illustration of S1 domain of KCNQ1 and KCNE1 indicating the region that was tested for cross-linking, as shown by green (KCNE1 residues) and red (KCNQ1 residues) dots. The numbers represent amino acid position. The dashed line above KCNQ1 indicates continuation of the channel. (B and C) Sample immunoblots are shown for the indicated pairs of Cys mutants of KCNQ1 and KCNE1. KCNQ1 is shown as a red signal and KCNE1 is shown as a green signal. The merged red and green signals indicate the cross-linked KCNQ1-KCNE1 band, which is shown as a yellow signal. The samples in the right lanes were reduced with 10 mM DTT in sample buffer. (B) Bar graph showing the percentage of spontaneous cross-linking for S140C with KCNE1 residues 40–51 ($n = 3$–6). (C) Bar graph showing the percentage of spontaneous cross-linking for V141C with KCNE1 residues 40–51 ($n = 4$–11). Calculations were based on the intensities of the bands, as described in Materials and methods. Data are shown as mean ± SEM (error bars). * and #, $P < 0.05$.

Cross-linking was determined by the percentage of cross-linked protein versus total protein (Fig. S3), and then plotted for the 24 cysteine pairs tested (Fig. 4, B and C). Sample immunoblots are shown for cross-linking results obtained from S140C and V141C, in the absence and presence of a reducing agent, DTT. For S140C

and each of 12 KCNE1 Cys mutants tested, disulfide bond formation was <10% (Fig. 4 B). This result suggests that S140 is not close enough to form contacts with KCNE1. To ensure that this residue was available to cross-link to Cys-KCNE1 residues, we verified its accessibility by testing the reactivity of the S140C residue with a membrane-impermeant MTS reagent (Fig. S2). In contrast, there is a high degree of disulfide bond formation between V141C and two Cys mutants on KCNE1: E43C and A44C. V141C/E43C exhibited 35 ± 4.3% cross-linking, whereas V141C/A44C exhibited 78 ± 2.4% cross-linking (Fig. 4 C); this is comparable to the high degree of cross-linking that was found for the extracellular flanks between KCNE1 and the S1 and S6 domains two KCNQ1 subunits (Chung et al., 2009).

Functional consequences of cross-link V141C/A44C reveal minor changes in channel function

Examination of the functional consequences of the cross-linking constructs revealed that substitution of a Cys at position 141 did not alter activation but slowed deactivation, which is in agreement with previous oocyte recordings (Restier et al., 2008). The single cysteine substituted KCNE1 (Cys-KCNE1) mutations at positions 43 and 44 did not alter function when coexpressed with WT KCNQ1 (Fig. S5). When V141C was coexpressed with A44C, the impact of cross-linking was minor; there was a further slight slowing of deactivation, in comparison to V141C alone, and no change in activation (Fig. S4). Reduction of the cross-link with DTT shifted the voltage dependence of activation (V141C/A44C [−DTT]: $V_{1/2} = 34.9 ± 2.7$ mV, $n = 5$; vs. V141C/ A44C (+DTT): $V_{1/2} = 46.3 ± 2.9$ mV, $n = 5$, $P < 0.05$) and caused a slight, statistically insignificant, speeding of deactivation (V141C/A44C (−DTT): $\tau_{deact} = 1.08 ± 0.06$ s, $n = 5$; vs. V141C/A44C (+DTT): $\tau_{deact} = 0.82 ± 0.21$ s, $n = 5$, $P > 0.05$). Both of these effects, however, are consistent with the effect of DTT alone in the WT KCNQ1 channel or in single Cys-KCNQ1 or single Cys-KCNE1 constructs, and therefore are likely independent of the reduction of the cross-link (Fig. S5; Chung et al., 2009). This result suggests that cross-linking of KCNQ1 V141C to KCNE1 likely does not perturb the native conformation of the channel, which suggests that V141, but not S140, is oriented toward KCNE1 in native channels.

Functional impact of KCNE1's location within a heterozygous KCNQ1 channel

Having shown evidence for the differential dependence of S140G and V141M mutations on the presence of KCNE1, we next turned to the question of whether or not the location of assembled KCNE1 subunits relative to mutation-containing S1 helices impacts the disease phenotype. Our previous results suggest that a direct physical interaction between KCNQ1 V141M and KCNE1 is required for the disease-associated phenotype. To further test this hypothesis, we constructed a tandem channel
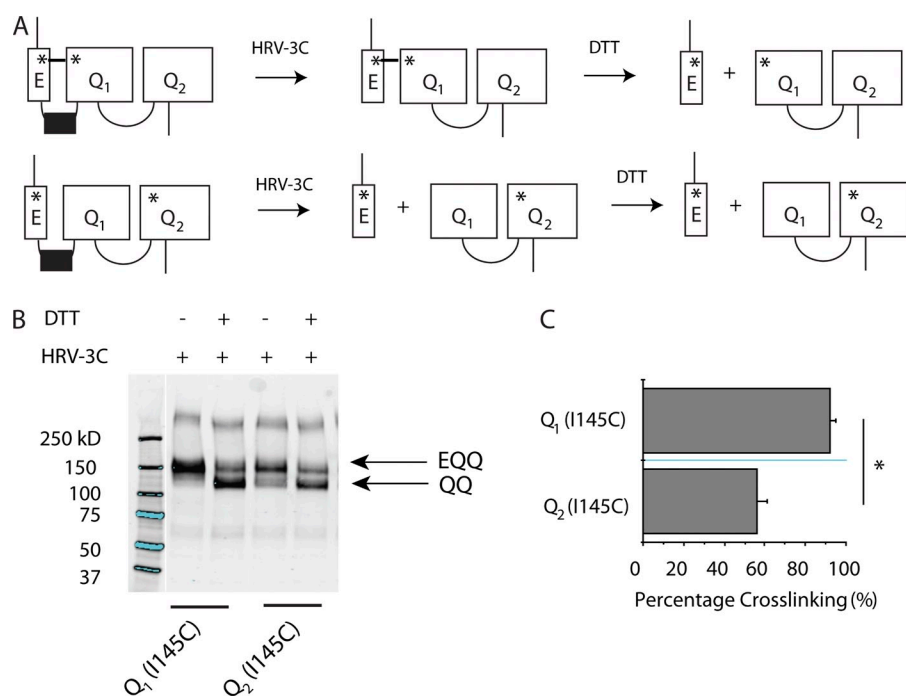
Figure 5. KCNE1 preferentially assembles next to proximal KCNQ1 subunit in tandem EQQ construct. (A) Schematic illustration of EQQ tandem constructs with engineered cysteine mutations (shown as asterisks). (B) Sample immunoblot is shown for the channels containing a Cys mutation, I145C, engineered into either Q_1 or Q_2 subunits. KCNE1 contains a Cys mutation, K41C. The samples were treated with HRV-3C protease to cleave between KCNE1 and KCNQ1, and were reduced with 10 mM DTT in sample buffer, as indicated above the blot. The molecular weight marker is taken from the same immunoblot but two lanes of the original blot were omitted, and hence the splicing of the gel is indicated by the line separating lanes 1 and 2. (C) Bar graph showing the percentage of spontaneous cross-linking for constructs Q_1 (I145C) or Q_2 (I145C) ($n = 4$). Calculations were based on the intensities of the bands, as described in Materials and methods. Data are shown as mean ± SEM (error bars). *, P < 0.05.

containing KCNE1 tethered to two KCNQ1 subunits (EQQ; Fig. 5 A), which has been used in previous KCNQ1 studies (Wang et al., 1998; Nakajo et al., 2010).

We first wanted to test if, in channels formed with this construct, KCNE1 preferentially assembles next to the S1 helix of a specific KCNQ1 subunit. We therefore engineered K41C into KCNE1 and I145C into either the proximal or distal KCNQ1 subunit of the linked EQQ construct, where two endogenous cysteines have been removed as in Chung et al. (2009). KCNE1 K41C has previously been shown to spontaneously cross-link to KCNQ1 I145C (Chung et al., 2009). To visualize cross-linking, we also engineered an HRV-3C protease site into the linker between KCNE1 and proximal KCNQ1 subunit (Fig. 5 A; Liu et al., 2008a). Fig. S6 shows that proteolysis of the introduced HRV-3C site is complete.

After isolating channels expressed at the cell surface, we applied protease to cleave KCNE1 from the KCNQ1-KCNQ1 dimer (QQ). If a cross-link occurs between KCNE1 and the proximal or distal KCNQ1, the EQQ band will remain after protease treatment. Subsequent treatment with DTT will reduce this cross-link, leaving just the KCNQ1-KCNQ1 dimer. As shown in Fig. 5, when I145C is present in the proximal KCNQ1 subunit, we find ∼90% cross-linking (Fig. 5, B and C). In contrast, when I145C is introduced into the distal KCNQ1 subunit, we find significantly less (∼50%) cross-linking. These results strongly suggest that in our tandem EQQ construct, KCNE1 preferentially assembles next to the S1 helix of the proximal KCNQ1 subunit.

We next functionally characterized tandem constructs containing the V141M mutation in either the proximal

or distal KCNQ1 subunit (Fig. 6 A). We find that when V141M is present in the proximal KCNQ1 subunit, deactivation is much slower than WT EQQ channels (Fig. 6 B). In contrast, when the V141M mutation is introduced into the distal KCNQ1 subunit, deactivation is not significantly different from WT EQQ channels (Fig. 6 C). These results indicate that for the V141M mutation, the position of KCNE1 relative to the mutation-containing S1 helix is critical to its disease phenotype and that a direct physical interaction between KCNE1 and V141M underlies the defect in channel deactivation.

Based on our data with KCNQ1 S140G monomers with and without KCNE1, it is unclear whether or not the more severe phenotype of KCNQ1 S140G channels in the presence of KCNE1 was also dependent on a direct interaction between KCNE1 and an S140G-containing S1 helix. To test this, we placed the S140G mutation in the proximal and distal KCNQ1 subunit of the EQQ tandem construct to see the effect of KCNE1-S140G proximity on channel function. As shown in Fig. 6 (D–E), while the deactivation of tandem channels containing S140G in the distal KCNQ1 subunit is significantly slowed, there is a significant additional effect on deactivation with S140G in the proximal KCNQ1 subunit, next to the assembled KCNE1. This suggests that a direct physical interaction between KCNE1 and the S140G-containing KCNQ1 S1 has a functional impact on the expression of a more severe deactivation phenotype. Collectively, our results with tandem EQQ constructs support a hypothesis that the relative expression and assembly of KCNE1 in heterozygous patients harboring V141M and S140G will affect the expression of the disease-causing channel phenotype.

Chan et al.   141

Figure 6. Intersubunit location of KCNE1 impacts functional consequences of KCNQ1 mutations. (A) Schematic illustration of EQQ tandem constructs: WT EQQ and AF mutations in the proximal (Q_1) or distal (Q_2) subunit (mutation represented as closed circles). (B) Representative tail current traces from cells expressing Q_1 V141M and Q_2 V141M EQQ constructs. The gray line indicates WT EQQ condition and the broken line indicates zero current. (C) Deactivation time constant (tau) obtained at -120 mV from single exponential fits to tail currents after conditioning pulses ($+20$ mV, 2 s). (D) Representative tail current traces from cells expressing Q_1 S140G and Q_2 S140G EQQ constructs. The gray line indicates WT EQQ condition and the broken line indicates zero current. (E) Deactivation time constant (tau) obtained at -120 mV from single exponential fits to tail currents after conditioning pulses ($+20$ mV, 2 s). For current traces (B and D), the vertical scale is 50 pA/pF and the horizontal scale is 0.5 s. Data are expressed as mean ± SEM (error bars). *, $P < 0.05$.
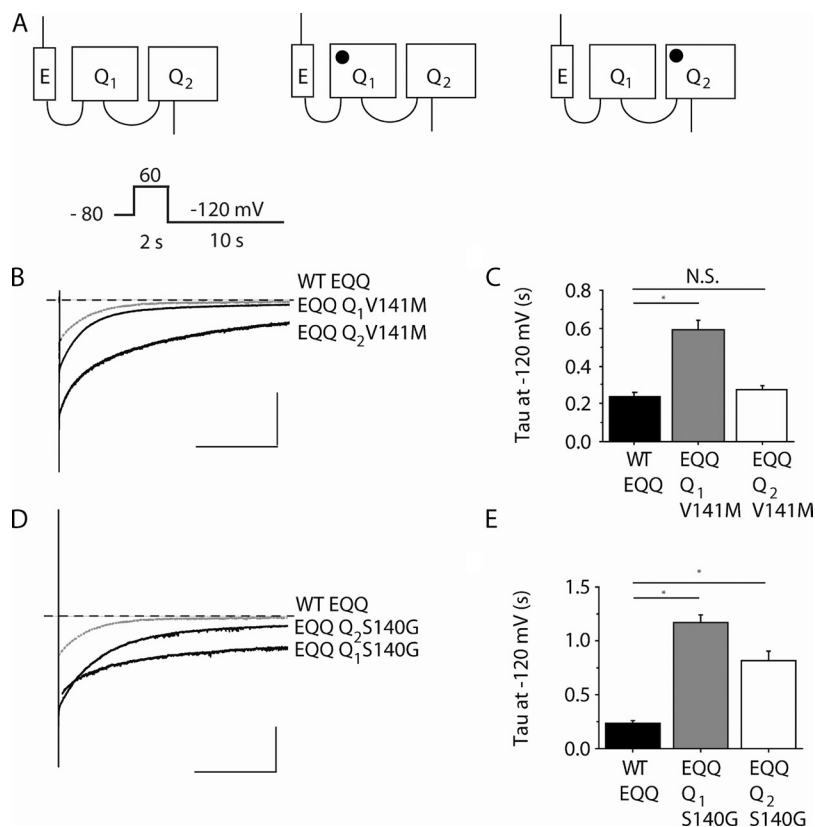
DISCUSSION

We find that KCNE1 plays a critical role in distinguishing two effects underlying the atrial fibrillation–associated KCNQ1 mutations S140G and V141M. Although both mutations disrupt deactivation in the presence of KCNE1, our experiments establish that S140G is able to slow channel deactivation in the absence of this subunit. We find that the V141M mutation in the KCNQ1 subunit alone is indistinguishable from the WT KCNQ1 subunit, confirming previous studies that this mutant phenotype requires the presence of KCNE1 (Hong et al., 2005). The marked impact of KCNE1 on deactivation of the V141M channel occurs despite the fact that there is no effect of the mutation on WT KCNQ1 homomeric channel function. This indicates an important role for KCNE1 in determining the disease phenotype of the V141M assembled channels.

Based on our functional experiments, biochemical cross-linking was performed to establish a structural basis for the differential KCNE1 dependence of these two mutant phenotypes. KCNE1 has previously been shown by spontaneous disulfide cross-linking to be positioned in the I_{Ks} channel in a manner that allows KCNE1 communication with S1 and S6 of different KCNQ1 subunits (Xu et al., 2008; Chung et al., 2009). Our cross-linking results build onto this placement of KCNE1 within the assembled channel. We demonstrate that V141C, but not S140C, spontaneously cross-links with cysteines

introduced in KCNE1 at positions 43 and 44. These results reveal a specific orientation of S1 whereby V141 is in close proximity to KCNE1, which is consistent with the KCNQ1 structural model (Fig. 7; Kang et al., 2008). With this positioning, it is clear why there is such a dramatic effect on channel function when KCNQ1 with the V141M mutation is assembled in the tetrameric channel in the presence of KCNE1. In the absence of KCNE1, it is likely that the V141 residue is not close to any region of the channel where it could affect channel function, which is in agreement with this mutation having no functional impact on KCNE1-free homomeric KCNQ1 channels. However, S140 is the neighboring residue on the S1 α helix, and its position can be inferred to be rotated back toward the S2-S4 helices within its own subunit. Thus, it is not in a favorable position to form cross-links with KCNE1 residues, but points in a direction that would allow it to impact the environment where S2 and S4 are located (Fig. 7 B). This prediction is consistent with our functional results showing that mutation of the S140 residue alone is sufficient to slow deactivation of homomeric KCNQ1 channels in the absence of KCNE1.

The functional consequences of the cross-link at V141C/A44C and V141C/E43C were observed to be minor, which indicates that cross-linking does not perturb the native conformation of the channel; consequently, these residues are likely in a relatively fixed position in the native state of the channel. Collectively,
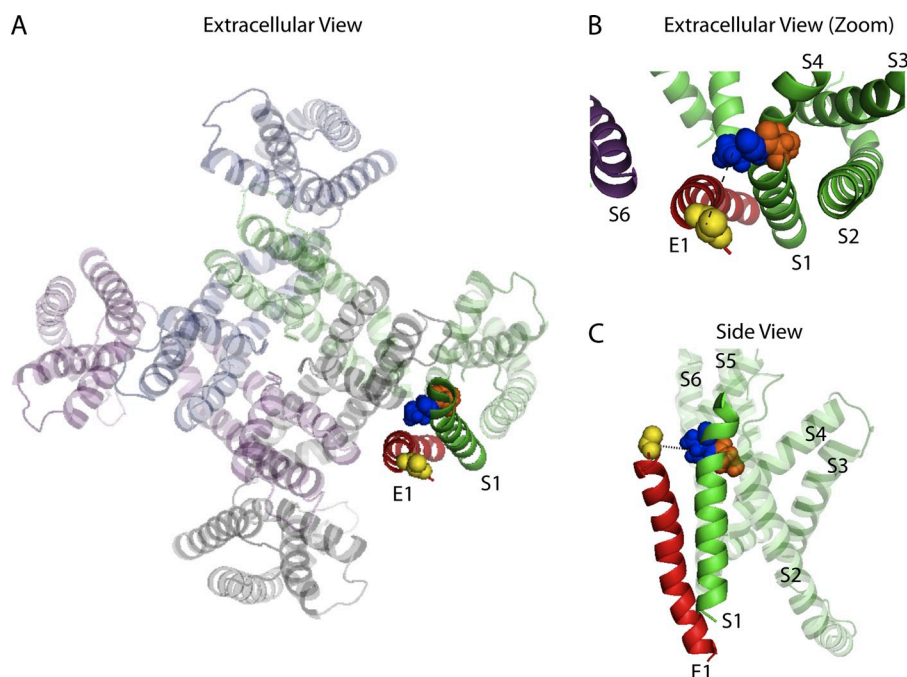
Figure 7. Predicted orientation of S1 KCNQ1 relative to KCNE1. (A) Extracellular view of KCNQ1 tetramer and KCNE1 transmembrane domain in the open state from Kang et al. (2008). (B) Extracellular view of KCNE1 (red) and S1 KCNQ1 (green) from Kang et al. (2008). V141 (blue) and S140 (orange) in S1 KCNQ1 are in space-fill representations. V141 points toward KCNE1, whereas S140 points toward S2–S4 domains of the same KCNQ1 subunit (gray). (C) Side view of KCNE1 and a single subunit of KCNQ1 taken from the Kang et al. (2008) open state model.

our results suggest an important region of proximity between the N-terminal end of KCNE1, near the transmembrane region and the extracellular end of KCNQ1 S1, that is particularly important in controlling deactivation kinetics of the KCNQ1/KCNE1 assembled channel. Based on these results, we propose that this KCNE1–KCNQ1 S1 interaction may mediate the KCNE1-induced changes in WT KCNQ1 deactivation.

The role of KCNE1 subunit assembly in channel gating was demonstrated using fusion constructs in which a KCNE1 subunit was positioned close to one KCNQ1 subunit but not to another KCNQ1 subunit. Using the results from our functional data characterizing the AF-associated mutations, S140G and V141M, we were able to demonstrate that the intersubunit location in the heteromultimeric channel is critical in translating the α subunit mutation into altered channel function. This is of particular relevance for congenital human disease in which heterozygote mutation carriers also carry one copy of WT KCNQ1. The requirement of KCNE1 for the most severe phenotype observed with these inherited mutations raises the interesting and important question of whether the pathological phenotype of these mutations may depend on the relative expression of KCNE1 in the heart and the resulting stoichiometry of KCNE1 in these channels. The tandem construct experiments in Figs. 5 and 6 further strengthen this possibility, as the data show that the location of KCNE1 relative to a mutant KCNQ1 in the assembled channel is critical in determining the severity of the channel defect. Mutation carriers in the S140G family have varied clinical phenotypes from no effect on AF to mild long QT (Chen et al., 2003). Whether the stoichiometric ratio of KCNE1 to KCNQ1

is fixed at 2:4, as suggested by the work of the Kobertz group (Morin and Kobertz, 2008), or variable, as suggested by recent single molecule imaging experiments (Nakajo et al., 2010); our work would strongly suggest a mandatory proximity of KCNQ1 to a nearby KCNE1 subunit, especially in the case of V141M, if the assembled channel is to be characterized by the key pathological phenotype: markedly slowed deactivation. In heterozygote patients, the number of KCNQ1 subunits carrying the disease-causing mutation will vary from one to four in assembled channels, and thus alter the potential contributions of KCNE1/KCNQ1 interactions underlying arrhythmia risk. Similarly, if in fact KCNE1/KCNQ1 stoichiometry is variable and may even vary during disease (Mustapha et al., 2007), then the severity of the disease phenotype, either for S140G or V141M mutation carriers, will be highly variable. Further, by this mechanism, chamber-specific variation in KCNE1 (Soma et al., 2011) may well play a role in these mutations' predominant effect occurring in the atria.

In this study, we find that neighboring AF mutations in KCNQ1 arrive at the same channel defect by two different pathways. For the S140G mutation, there are dramatic effects on KCNQ1 channel deactivation in the absence of KCNE1. However, for the V141M mutation, no change in channel behavior is observed without KCNE1 present. Biochemical cross-linking data also demonstrate that residue V141 is positioned close to and is facing KCNE1, revealing a specific orientation of the KCNQ1 and KCNE1 subunits. We also demonstrate that the location of KCNE1 within a heterozygous channel complex impacts the severity of the mutant phenotype. Collectively, our results implicate a physiologically important

interaction between KCNE1 and KCNQ1 S1 that affects the rate of channel deactivation in a mutation-specific manner, underlying heritable cardiac disease.

REFERENCES

Barhanin, J., F. Lesage, E. Guillemare, M. Fink, M. Lazdunski, and G. Romey. 1996. K(V)LQT1 and lsK (minK) proteins associate to form the I(Ks) cardiac potassium current. *Nature.* 384:78–80. http://dx.doi.org/10.1038/384078a0

Bellocq, C., A.C. van Ginneken, C.R. Bezzina, M. Alders, D. Escande, M.M. Mannens, I. Baró, and A.A. Wilde. 2004. Mutation in the KCNQ1 gene leading to the short QT-interval syndrome. *Circulation.* 109:2394–2397. http://dx.doi.org/10.1161/01.CIR.0000130409.72142.FE

Chen, Y.H., S.J. Xu, S. Bendahhou, X.L. Wang, Y. Wang, W.Y. Xu, H.W. Jin, H. Sun, X.Y. Su, Q.N. Zhuang, et al. 2003. KCNQ1 gain-of-function mutation in familial atrial fibrillation. *Science.* 299:251–254. http://dx.doi.org/10.1126/science.1077771

Chung, D.Y., P.J. Chan, J.R. Bankston, L. Yang, G. Liu, S.O. Marx, A. Karlin, and R.S. Kass. 2009. Location of KCNE1 relative to KCNQ1 in the I(KS) potassium channel by disulfide cross-linking of substituted cysteines. *Proc. Natl. Acad. Sci. USA.* 106:743–748. http://dx.doi.org/10.1073/pnas.0811897106

Das, S., S. Makino, Y.F. Melman, M.A. Shea, S.B. Goyal, A. Rosenzweig, C.A. Macrae, and P.T. Ellinor. 2009. Mutation in the S3 segment of KCNQ1 results in familial lone atrial fibrillation. *Heart Rhythm.* 6:1146–1153. http://dx.doi.org/10.1016/j.hrthm.2009.04.015

Hong, K., D.R. Piper, A. Diaz-Valdecantos, J. Brugada, A. Oliva, E. Burashnikov, J. Santos-de-Soto, J. Grueso-Montero, E. Diaz-Enfante, P. Brugada, et al. 2005. De novo KCNQ1 mutation responsible for atrial fibrillation and short QT syndrome in utero. *Cardiovasc. Res.* 68:433–440. http://dx.doi.org/10.1016/j.cardiores.2005.06.023

Kang, C., C. Tian, F.D. Sönnichsen, J.A. Smith, J. Meiler, A.L. George Jr., C.G. Vanoye, H.J. Kim, and C.R. Sanders. 2008. Structure of KCNE1 and implications for how it modulates the KCNQ1 potassium channel. *Biochemistry.* 47:7999–8006. http://dx.doi.org/10.1021/bi800875q

Kurokawa, J., L. Chen, and R.S. Kass. 2003. Requirement of subunit expression for cAMP-mediated regulation of a heart potassium channel. *Proc. Natl. Acad. Sci. USA.* 100:2122–2127. http://dx.doi.org/10.1073/pnas.0434935100

Liu, G., S.I. Zakharov, L. Yang, S.X. Deng, D.W. Landry, A. Karlin, and S.O. Marx. 2008a. Position and role of the BK channel alpha subunit S0 helix inferred from disulfide crosslinking. *J. Gen. Physiol.* 131:537–548. http://dx.doi.org/10.1085/jgp.200809968

Liu, G., S.I. Zakharov, L. Yang, R.S. Wu, S.X. Deng, D.W. Landry, A. Karlin, and S.O. Marx. 2008b. Locations of the beta1 transmembrane helices in the BK potassium channel. *Proc. Natl. Acad. Sci. USA.* 105:10727–10732. http://dx.doi.org/10.1073/pnas.0805212105

Lundby, A., L.S. Ravn, J.H. Svendsen, S.P. Olesen, and N. Schmitt. 2007. KCNQ1 mutation Q147R is associated with atrial fibrillation and prolonged QT interval. *Heart Rhythm.* 4:1532–1541. http://dx.doi.org/10.1016/j.hrthm.2007.07.022

Marx, S.O., J. Kurokawa, S. Reiken, H. Motoike, J. D'Armiento, A.R. Marks, and R.S. Kass. 2002. Requirement of a macromolecular signaling complex for beta adrenergic receptor modulation of the KCNQ1-KCNE1 potassium channel. *Science.* 295:496–499. http://dx.doi.org/10.1126/science.1066843

Morin, T.J., and W.R. Kobertz. 2008. Counting membrane-embedded KCNE beta-subunits in functioning K+ channel complexes. *Proc. Natl. Acad. Sci. USA.* 105:1478–1482. http://dx.doi.org/10.1073/pnas.0710366105

Murai, T., A. Kakizuka, T. Takumi, H. Ohkubo, and S. Nakanishi. 1989. Molecular cloning and sequence analysis of human genomic DNA encoding a novel membrane protein which exhibits a slowly activating potassium channel activity. *Biochem. Biophys. Res. Commun.* 161:176–181. http://dx.doi.org/10.1016/0006-291X(89)91577-5

Mustapha, Z., L. Pang, and S. Nattel. 2007. Characterization of the cardiac KCNE1 gene promoter. *Cardiovasc. Res.* 73:82–91. http://dx.doi.org/10.1016/j.cardiores.2006.10.022

Nakajo, K., M.H. Ulbrich, Y. Kubo, and E.Y. Isacoff. 2010. Stoichiometry of the KCNQ1 - KCNE1 ion channel complex. *Proc. Natl. Acad. Sci. USA.* 107:18862–18867. http://dx.doi.org/10.1073/pnas.1010354107

Restier, L., L. Cheng, and M.C. Sanguinetti. 2008. Mechanisms by which atrial fibrillation-associated mutations in the S1 domain of KCNQ1 slow deactivation of IKs channels. *J. Physiol.* 586:4179–4191. http://dx.doi.org/10.1113/jphysiol.2008.157511

Sanguinetti, M.C., and N.K. Jurkiewicz. 1990. Two components of cardiac delayed rectifier K+ current. Differential sensitivity to block by class III antiarrhythmic agents. *J. Gen. Physiol.* 96:195–215. http://dx.doi.org/10.1085/jgp.96.1.195

Sanguinetti, M.C., M.E. Curran, A. Zou, J. Shen, P.S. Spector, D.L. Atkinson, and M.T. Keating. 1996. Coassembly of K(V)LQT1 and minK (IsK) proteins to form cardiac I(Ks) potassium channel. *Nature.* 384:80–83. http://dx.doi.org/10.1038/384080a0

Sesti, F., and S.A. Goldstein. 1998. Single-channel characteristics of wild-type IKs channels and channels formed with two minK mutants that cause long QT syndrome. *J. Gen. Physiol.* 112:651–663. http://dx.doi.org/10.1085/jgp.112.6.651

Soma, K., K. Nagaoka, M. Kuwahara, H. Tsubone, and K. Ito. 2011. Abundant expression of KCNE1 in the left ventricle of the miniature pig. *Heart Vessels.* 26:353–356. http://dx.doi.org/10.1007/s00380-010-0041-0

Splawski, I., J. Shen, K.W. Timothy, M.H. Lehmann, S. Priori, J.L. Robinson, A.J. Moss, P.J. Schwartz, J.A. Towbin, G.M. Vincent, and M.T. Keating. 2000. Spectrum of mutations in long-QT syndrome genes. KVLQT1, HERG, SCN5A, KCNE1, and KCNE2. *Circulation.* 102:1178–1185.

Tristani-Firouzi, M., and M.C. Sanguinetti. 1998. Voltage-dependent inactivation of the human K+ channel KvLQT1 is eliminated by association with minimal K+ channel (minK) subunits. *J. Physiol.* 510:37–45. http://dx.doi.org/10.1111/j.1469-7793.1998.037bz.x

Wang, W., J. Xia, and R.S. Kass. 1998. MinK-KvLQT1 fusion proteins, evidence for multiple stoichiometries of the assembled IsK channel. *J. Biol. Chem.* 273:34069–34074. http://dx.doi.org/10.1074/jbc.273.51.34069

Xu, X., M. Jiang, K.L. Hsu, M. Zhang, and G.N. Tseng. 2008. KCNQ1 and KCNE1 in the IKs channel complex make state-dependent contacts in their extracellular domains. *J. Gen. Physiol.* 131:589–603. http://dx.doi.org/10.1085/jgp.200809976